ACS SENSORS

pubs.acs.org/acssensors

Article

Interrogation of Electrochemical Aptamer-Based Sensors via Peak-to-Peak Separation in Cyclic Voltammetry Improves the Temporal Stability and Batch-to-Batch Variability in Biological Fluids

Miguel Aller Pellitero, Samuel D. Curtis, and Netzahualcóyotl Arroyo-Currás*

Cite This: *ACS Sens.* 2021, 6, 1199–1207

Read Online

ACCESS | Metrics & More | Article Recommendations | Supporting Information

ABSTRACT: Electrochemical, aptamer-based (E-AB) sensors support continuous, real-time measurements of specific molecular targets in complex fluids such as undiluted serum. They achieve these measurements by using redox-reporter-modified, electrode-attached aptamers that undergo target binding-induced conformational changes which, in turn, change electron transfer between the reporter and the sensor surface. Traditionally, E-AB sensors are interrogated via pulse voltammetry to monitor binding-induced changes in transfer kinetics. While these pulse techniques are sensitive to changes in electron transfer, they also respond to progressive changes in the sensor surface driven by biofouling or monolayer desorption and, consequently, present a significant drift. Moreover, we have empirically observed that differential voltage pulsing can accelerate monolayer desorption from the sensor surface, presumably via field-induced actuation of aptamers. Here, in contrast, we demonstrate the potential advantages of employing cyclic voltammetry to measure electron-transfer changes directly. In our approach, the target concentration is reported via changes in the peak-to-peak separation, ΔE_P, of cyclic voltammograms. Because the magnitude of ΔE_P is insensitive to variations in the number of aptamer probes on the electrode, ΔE_P-interrogated E-AB sensors are resistant to drift and show decreased batch-to-batch and day-to-day variability in sensor performance. Moreover, ΔE_P-based measurements can also be performed in a few hundred milliseconds and are, thus, competitive with other subsecond interrogation strategies such as chronoamperometry but with the added benefit of retaining sensor capacitance information that can report on monolayer stability over time.

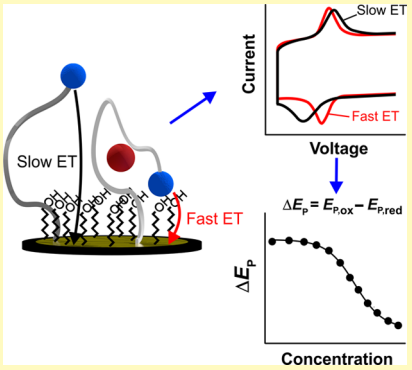

KEYWORDS: *aptamer, biosensor, cyclic voltammetry, undiluted serum, drift correction*

Electrochemical, aptamer-based (E-AB) sensors[1,2] are analytical platforms that achieve continuous monitoring of specific molecular targets in vivo.[3] E-AB sensors present an architecture consisting of three elements (Figure 1A):[4,5] (1) a self-assembled monolayer (SAM) of target-binding, alkanethiol-functionalized nucleic acid aptamers, (2) an electrode-blocking SAM of alkanethiols to prevent undesired electrochemical reactions and confer biocompatibility to the electrode surface, and (3) a redox reporter sensitive to target-binding events. The redox reporter, typically methylene blue (MB),[6,7] is attached to the terminal end of the aptamer, opposite to the electrode attachment terminus. In the presence of a target, aptamer molecules reversibly undergo binding-induced conformational changes that presumably bring the reporter closer to the electrode surface,[8] causing a change in the electron-transfer rate between the reporter and the electrode, which can be easily measured electrochemically (Figure 1B).[4] Aptamer binding in E-AB sensors is at dynamic equilibrium, reversibly switching between bound and unbound states at rates of milliseconds.[9] This behavior makes E-AB sensors ideal for continuous monitoring applications. Moreover, because their working principle mimics the binding-induced conformational changes seen in naturally occurring chemoreceptors in the body,[10] E-AB sensors tolerate prolonged measurements in complex matrices such as unprocessed biological fluids.[11−13]

E-AB sensors can be successfully interrogated via chronoamperometry,[14] differential pulse techniques such as square wave voltammetry and differential pulse voltammetry,[15] alternating current voltammetry,[16] or electrochemical impedance spectroscopy.[17] Published reviews discuss the benefits and disadvantages of each of these interrogation techniques.[4,18,19] Ultimately, the choice of technique is determined by the final intended application of the E-AB sensor. For example, the simplicity of the voltage program in chronoamperometry is ideal for drift-free measurements at subsecond interrogation frequencies,[14,20] which may be needed for the

Received: November 24, 2020
Accepted: February 10, 2021
Published: February 18, 2021

https://dx.doi.org/10.1021/acssensors.0c02455
ACS Sens. 2021, 6, 1199–1207

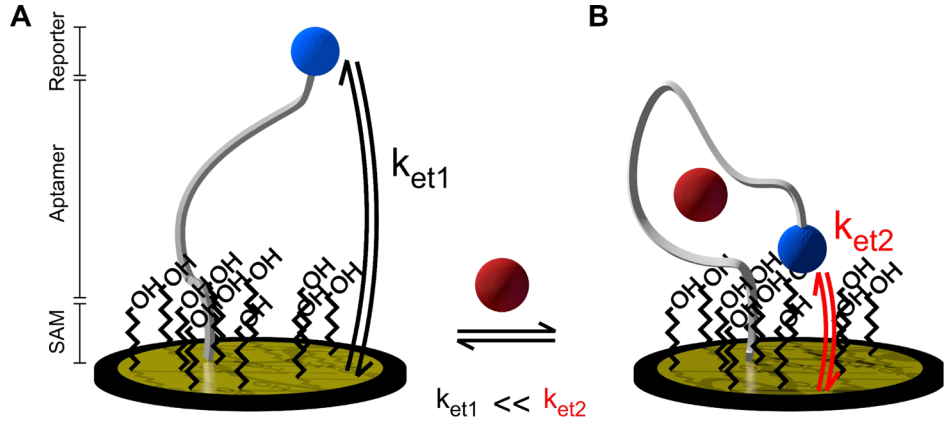

Figure 1. E-AB sensors undergo target binding-induced changes in electron-transfer kinetics of the redox reporter that can be monitored in real time via electrochemical interrogation. (A) In this work, we employed three different DNA aptamers modified at the 5′ terminus with alkanethiol linkers and at the 3′ terminus with the redox reporter MB. We codeposited these modified oligonucleotides with 6-mercapto-1-hexanol on the surface of gold electrodes via self-assembly. (B) In the presence of their target molecule, the aptamers undergo a conformational change that, presumably, brings the redox reporter closer to the electrode surface, increasing the electron-transfer rate.

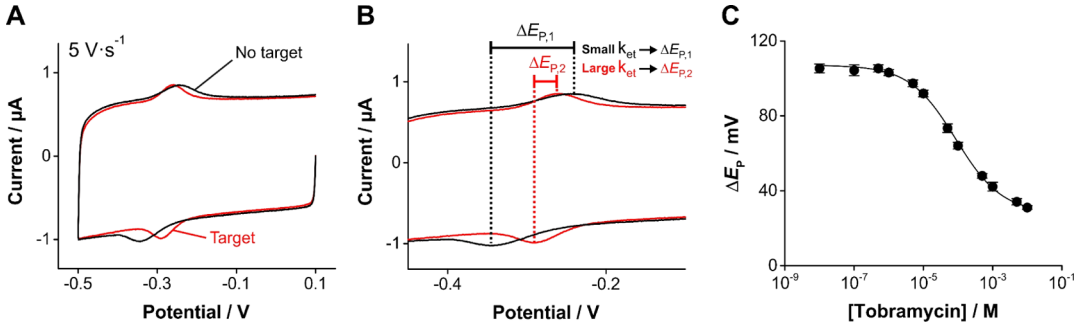

Figure 2. Target binding-induced changes in apparent electron-transfer rates of E-AB sensors can be monitored via ΔE_P. (A) When we interrogate tobramycin-detecting E-AB sensors using CV (at 5 V·s^{-1}), we observe a decrease in ΔE_P upon the addition of tobramycin (10 mM). (B) Same voltammograms as in (A) but zoomed-in relative to the *x*-axis show more clearly the change in electron-transfer rate (k_{et}) from $\Delta E_{P,1}$ to $\Delta E_{P,2}$, with $\Delta E_{P,2} < \Delta E_{P,1}$. (C) The magnitude of ΔE_P decreases monotonically with increasing target concentration. The solid line is a nonlinear fit to the Hill equation, resulting in a Hill coefficient $n = 1$ and $K_D = 80 \pm 7$ μM. Error bars represent the standard deviation between five electrodes. All measurements performed in 1× phosphate-buffered saline (PBS).

study of fast biological processes such as the neurotransmitter modulation in the brain.[5] Electrochemical impedance, in contrast, offers the convenience of interrogating E-AB sensors in a label-free manner, without using a redox reporter.[21] However, the vast majority of the reported E-AB sensors have been interrogated by pulse techniques and, in particular, by square wave voltammetry.[19,22] This widespread use likely arose because pulsed techniques differentially remove currents originating from charging the electrode−electrolyte double layer, significantly improving the signal-to-noise ratio of E-AB measurements. Yet, pulsed techniques also remove valuable electrochemical information regarding the sensor stability (e.g., the capacitive current reports on monolayer stability) and, as we show here, differential voltage pulsing also strains the E-AB interface causing a faster loss of the signal.

Cyclic voltammetry (CV) is frequently used for the surface characterization of E-AB sensors, as this technique provides valuable information regarding the monolayer stability[22] (by proxy of double-layer capacitance) and surface coverage of the redox reporter-modified aptamer (from faradaic peak areas).[23] However, CV is not commonly used for the direct interrogation of E-AB sensors, in part because sensors with defective blocking monolayers or redox reporter-modified aptamers with slow electron-transfer kinetics present large capacitive currents that can hide the faradaic waves of MB, resulting in low signal-to-noise E-AB measurements.[19] Moreover, for many E-AB sensors, CV peak currents do not change significantly with increasing target concentrations. To overcome these limitations, here we introduce a general CV-based interrogation approach that employs voltammogram peak-to-peak separation (ΔE_P) to directly measure binding-induced changes in the apparent electron-transfer kinetics of E-AB sensors. We demonstrate that the voltage program used in CV is less damaging to the E-AB interface over time and that ΔE_P-based interrogation can achieve E-AB measurements with a significantly reduced batch-to-batch and day-to-day variability relative to the benchmark square wave voltammetry.

RESULTS AND DISCUSSION

The magnitude of ΔE_P in CV can be used to interrogate changes in the apparent electron-transfer kinetics of E-AB sensors. ΔE_P is affected by a mass-transfer (diffusional) component related to the conformation switching behavior of aptamers;[24] thus, measured changes in ΔE_P reflect target-binding induced changes in the aptamer conformation. We first illustrate this effect employing tobramycin-detecting E-AB sensors (Figure 2), which have been extensively validated in the literature and represent a well-understood model

https://dx.doi.org/10.1021/acssensors.0c02455
ACS Sens. 2021, 6, 1199−1207

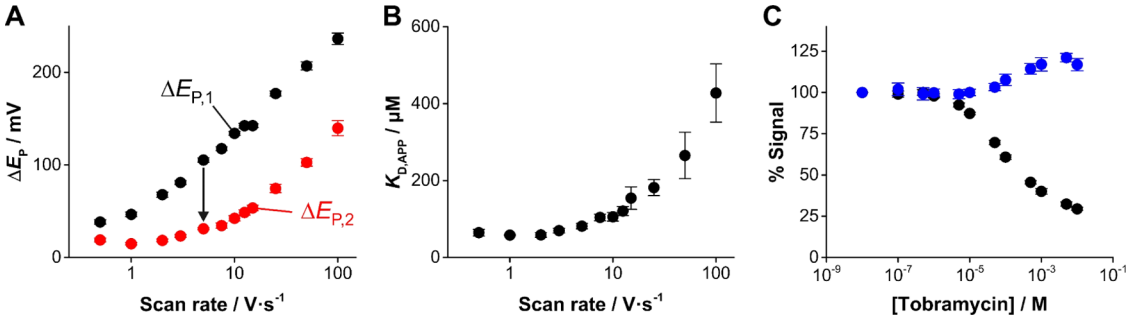

Figure 3. E-AB sensor gain and sensitivity based on ΔE_P are a strong function of the voltage scanning rate. (A) We illustrate this effect by showing ΔE_P values in the absence (black circles, $\Delta E_{P,1}$) and presence (red circles, $\Delta E_{P,2}$) of saturating concentrations of tobramycin (10 mM) at increasing voltage scanning rates. Note that, although ΔE_P increases with the increasing scanning rate in both cases, it does not do so with the same correlation function. Thus, CV scanning rates ranging between 5 and 10 V s^{-1} produce the largest signal change based on ΔE_P. (B) Dose−response curves built from ΔE_P measurements result in apparent aptamer dissociation constants that strongly depend on the CV scanning rate. Interrogating tobramycin-detecting E-AB sensors at CV scanning rates between 5 and 10 V s^{-1} achieve the most sensitive measurements (lowest apparent K_D) with the largest overall signal gain. (C) Side-by-side comparison of sensors interrogated by CV using voltammetric peak heights, I_P (blue circles) vs ΔE_P (black circles) to illustrate that ΔE_P achieves a 3-fold improvement in signal gain relative to I_P, albeit with the opposite sign. Error bars represent the standard deviation between the five electrodes. All measurements were performed in 1× PBS.

system.[3,14,25] In these E-AB sensors, interrogation by CV in the absence of a target and at voltage scanning rates of ∼1−10 V s^{-1} results in voltammograms with a ΔE_P ∼100 mV (Figure 2A). However, the addition of a saturating concentration of tobramycin (10 mM) causes a significant increase in the apparent electron-transfer kinetics with a concomitant decrease in ΔE_P to ∼30 mV (Figure 2A,B). Similar measurements at varying tobramycin concentrations can be translated into dose−response curves (Figure 2C). The dissociation constant estimated by extrapolating the mid-point of these dose−response curves to the *x*-axis, K_D ∼80 μM, is within a factor of 3−4 relative to previously reported K_D measurements based on chronoamperometric (K_D ∼30 μM) and differential pulse measurements (K_D ∼20 μM).[14] This difference in the magnitude of the apparent K_D may be due in part to differences in the aptamer packing density used for the measurements performed in Figure 2 (∼0.9 pmol·cm^2, from a 500 nM DNA solution), relative to those used in previously published reports (<0.7 pmol·cm^2, from a 200 nM DNA solution), and in part to the different electrode geometry; this work employed gold disc macroelectrodes versus microelectrode wires used in prior works by Plaxco and colleagues.[14]

The aptamer packing density is known to affect the signaling output[26,27] and electron-transfer kinetics.[28,29] of DNA-based sensors in general. Thus, to further investigate the effect of the aptamer packing density on ΔE_P, we prepared three batches of four tobramycin-binding E-AB sensors using DNA deposition solutions at concentrations of 100, 500, and 1000 nM. The resulting packing densities calculated via integration of the area under the MB faradaic redox wave in the presence of saturating tobramycin levels are reported in Table S1. Interrogating these sensors, we observed aptamer densities ranging between 0.5 and 1.0 pmol·cm^2, producing a maximum variability in the magnitude of ΔE_P of ∼10%. This result implies that, in the range considered, the effect of the aptamer packing density on the magnitude of ΔE_P, and thus the signaling output of our approach, is not significant. In contrast, the variability in I_P is more acute, observing a drop of ∼60% between the higher and lower packing densities. All measurements performed in the following figures used aptamer monolayers with packing densities = 0.9 ± 0.1 pmol·cm^2.

The magnitude of ΔE_P in cyclic voltammograms of E-AB sensors can be a strong function of the voltage scanning rate. To investigate this effect, we interrogated a fresh batch of tobramycin-detecting E-AB sensors at scanning rates ranging from 0.5 to 100 V s^{-1} in the presence and absence of saturating tobramycin concentrations (Figure 3A). At scanning rates <0.5 V s^{-1}, cyclic voltammograms presented a ΔE_P that closely approached 0 mV, as expected for an electrode-bound, quasireversible system such as the one considered here.[30] However, at faster scanning rates, the magnitude of ΔE_P progressively increased in both the presence or absence of tobramycin, albeit not with the same correlation function. This increase in ΔE_P occurred because the CV scanning rates became faster than the diffusional contribution arising from the conformation-switching behavior of aptamers (i.e., the measurement rate became faster than the apparent electron-transfer rate). Yet, because the addition of target moves the equilibrium in Figure 1 to the right (i.e., it accelerates electron transfer), $\Delta E_{P,2}$ is always smaller than $\Delta E_{P,1}$. Thus, the magnitude of ΔE_P can be effectively used to interrogate the electron-transfer state of tobramycin-detecting E-AB sensors, with the maximum signal change observed at scanning rates between 5 and 10 V s^{-1}.

As with all E-AB interrogation methods, there is a trade-off between the maximum signal gain observed by ΔE_P and the apparent dissociation constant of the sensors. To illustrate this, we measured dose−response curves as shown in Figure 2C at scanning rates ranging from 0.5 to 100 V s^{-1} (Figure S1). Then, we determined the apparent dissociation constant at each scanning rate by performing a nonlinear regression of the data sets using the Hill isotherm. The resulting graph of K_D versus voltage scanning rate (Figure 3B) shows a strong dependence on the scanning rate, with a significant deviation from the published K_Ds (determined by square wave voltammetry or chronoamperometry[14]) at scanning rates >10 V s^{-1}. Moreover, the shape of the voltammograms was distorted at fast scanning rates, preventing the accurate determination of ΔE_P (Figure S2). Thus, taking into consideration the results presented in Figure 3A,B, we determined that the best CV interrogation rate for tobramycin-detecting E-AB sensors was 5 V s^{-1}.

https://dx.doi.org/10.1021/acssensors.0c02455
ACS Sens. 2021, 6, 1199−1207

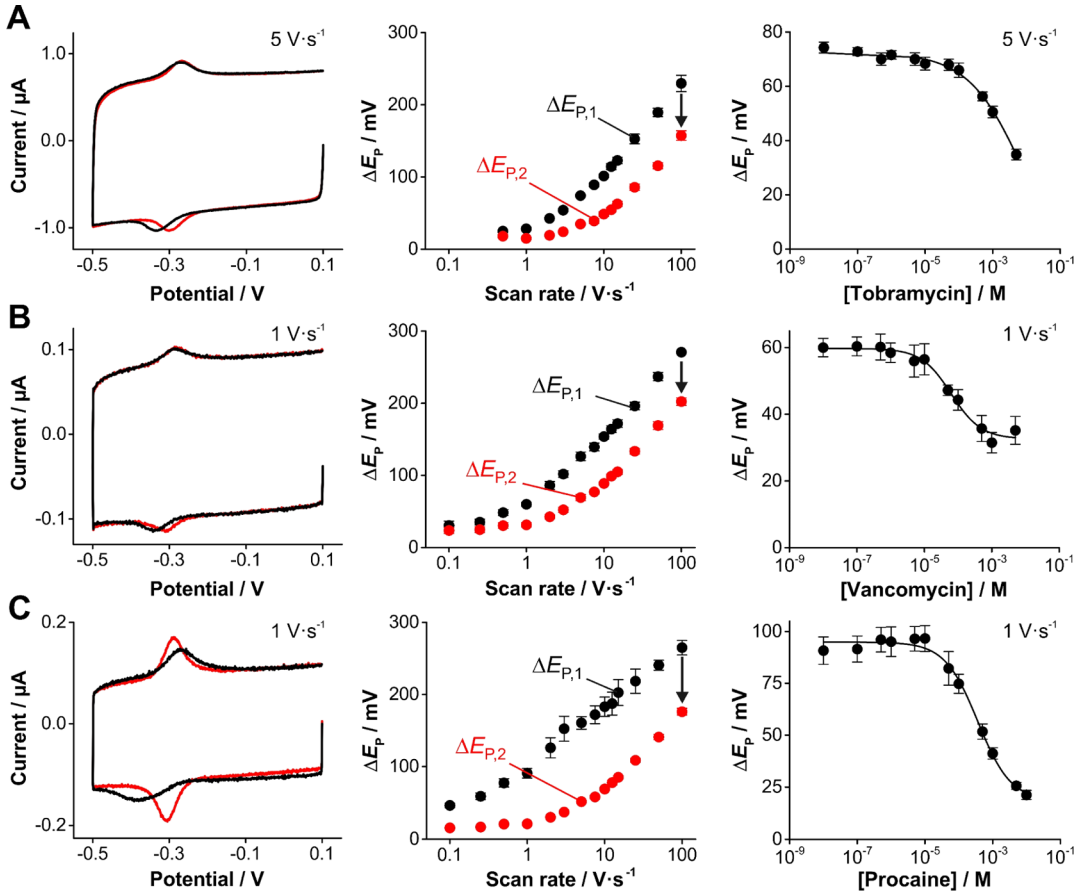

Figure 4. ΔE_P-based interrogation supports E-AB measurements irrespective of the aptamer used. We evaluated the general suitability of our method for E-AB sensing in undiluted serum by fabricating sensors using (A) tobramycin-, (B) vancomycin-, and (C) procaine-binding aptamers. Here, we show the performance of these sensors in undiluted serum when interrogated by CV. Left. Cyclic voltammograms measured in the absence (black trace) and presence (red trace) of a saturating target show significant differences in ΔE_P. Note that for tobramycin and vancomycin, we observed minimal change in I_P. However, voltammograms measured with the procaine sensor did show a significant change in I_P matching a broadening of the faradaic waves. Center. Scan rate dependency of each sensor to determine the region of maximum signal decrease between the unbound and bound states. Right. We use the scanning rate giving the best compromise between maximum signal change and low apparent K_D to build calibration curves for each analyte. Error bars represent the standard deviation between five electrodes. The calculated detection limit was 117 ± 4, 45 ± 6, and 60 ± 10 μM for the tobramycin, vancomycin, and procaine sensors, respectively. The precision of each sensor observed by this method can be found in Figure S5.

E-AB interrogation via ΔE_P achieves larger signal gains relative to the interrogation based on CV peak heights. To illustrate this point, we measured dose−response curves at the optimal voltage scanning rate of 5 V s^{-1} and compared the response based on voltammogram peak currents, I_P, at varying tobramycin concentrations relative to the proposed ΔE_P-based method (Figure 3C). To achieve a direct comparison between approaches, we calculated the relative change in signal at each concentration with respect to the signal measured in the absence of a target (this is common practice in the field).[14] By graphing I_P versus concentration, we observed a "signal-on" type of response, with I_P increasing to a plateau of 20% relative signal change at saturation. Using ΔE_P, in contrast, we observed a "signal-off" type of response, with ΔE_P decreasing by 80% relative signal change at saturation. From these results, we conclude that, on the one hand, ΔE_P achieves a larger signal gain (i.e., larger net signal change), thereby improving the sensitivity of CV-interrogated E-ABs. On the other hand, ΔE_P provides a signal-off response that is less desirable than the signal-on response achieved by monitoring I_P. Typically, the use of signal-off sensing is suboptimal for continuous monitoring in complex fluids, as matrix effects can induce signal decreases unrelated to fluctuations in target concentration that can be confounding during sensing. However, below we demonstrate that the ΔE_P-based interrogation of E-ABs achieves, in fact, superior stability than I_P-based interrogation methods with less batch-to-batch measurement variability in, for example, undiluted serum.

The enhanced signal gain seen with the ΔE_P-based interrogation can be explained by its strong correlation to electron-transfer kinetics. For diffusionless quasireversible systems, Laviron established that ΔE_P can be accurately used to determine the electron-transfer rate constants.[30] Although, technically, the E-AB system is not entirely diffusionless—previous works have demonstrated a diffusional contribution to the electrochemical response for DNA sequences longer that 10 nucleotides[24,31]—ΔE_P does directly reflect binding-induced changes in the apparent electron-transfer kinetics. Voltammetric peak currents, in contrast, are more reflective of the total number of electrons being transferred in the voltammetric sweep (i.e., total moles of reporter-modified aptamer) and not of electron-transfer rate. We experimentally demonstrate this for tobramycin-binding E-AB sensors by comparing side-by-side the behavior of ΔE_P and I_P in the absence and presence of

https://dx.doi.org/10.1021/acssensors.0c02455
ACS Sens. 2021, 6, 1199−1207

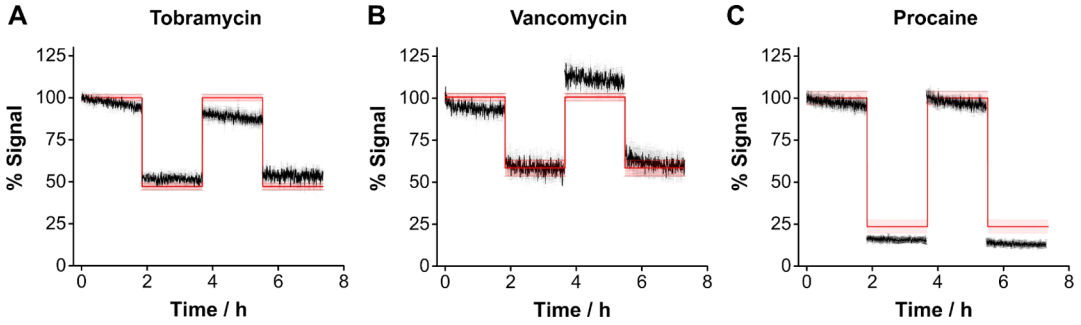

Figure 5. Serially interrogating E-AB sensors via ΔE_p supports second to subsecond monitoring of fluctuating target concentrations in real time. Here, we show serial ΔE_p measurements (black traces) recorded at (A) 5 V s^{-1} for tobramycin, (B) 1 V s^{-1} for vancomycin, and (C) 1 V s^{-1} for procaine. Using a voltage window of 600 mV (e.g., see Figure 2A), these scanning rates achieve measurements every 0.24, 1.2, and 1.2 s, respectively. To demonstrate the E-AB performance over time, in these panels we recorded measurements for 7 h alternating between 100% serum, and serum + target at a saturating concentration. To reveal the percentage contribution of drift to our measurements, we present the data as the relative change in signal with respect to the signal measured at the start of each experiment. We eliminated the effect of temperature fluctuations by maintaining the electrochemical cell at 25 °C using a water jacket and a temperature-controlled recirculation bath. We also continuously stirred the serum at ~100 rpms to avoid precipitation of solids from the serum. Red traces represent the expected relative signal change in the absence or presence of a target as given by our calibration curves from Figure 4. Error bars represent the standard deviation between the five electrodes.

a target and at various scanning rates (Figure S3). This analysis shows that, at the optimal voltage scanning rate of 5 V s^{-1}, challenging the E-AB sensors with target causes a more pronounced change in ΔE_p than in I_p. This effect is perhaps most emphasized at scanning rates <1 V s^{-1}, where I_p is completely insensitive to target additions (Figure S4).

ΔE_p-based interrogation of E-AB sensors supports molecular measurements in complex media such as undiluted serum. Moreover, the approach can be used to interrogate E-AB sensors detecting different molecular targets. We demonstrate these points here by interrogating sensors employing aptamers that bind to three structurally different therapeutics: the aminoglycoside tobramycin, the glycopeptide vancomycin, and the amino ester procaine (Figure 4). Using ΔE_p-based interrogation in an undiluted serum and mapping CV scan rates to identify the voltage sweep speed producing maximum change in ΔE_p, we observed that tobramycin-detecting E-AB sensors (Figure 4A) present a significant decrease in affinity relative to measurements performed in PBS (Figure 2C). Furthermore, the relative change in ΔE_p at 10 mM tobramycin was 30% less than the gain seen in PBS. Both of these effects were previously reported for serum tobramycin E-AB measurements performed by chronoamperometry, confirming that ΔE_p is not more prone to fouling than, for example, chronoamperometric current decay lifetimes.[14] Similarly, interrogating vancomycin-detecting sensors using ΔE_p (Figure 4B) resulted in serum calibration curves that did not differ in affinity relative to previous measurements performed in blood;[32] that is, the K_D remained at ~60 μM, with a total relative change in ΔE_p at saturating vancomycin concentrations of ~50%. Last, procaine-detecting E-AB sensors presented the largest change in ΔE_p, corresponding to a relative decrease of ~80% at saturating procaine concentrations (Figure 4C). Based on our calibration curve, the procaine-binding aptamer has a K_D of ~500 μM, slightly better than the affinity obtained by, for example, square wave voltammetry (K_D ~2 mM, Figure S6).

Because ΔE_p can rapidly respond to fluctuating target levels, our approach supports continuous molecular monitoring in complex fluids. We evaluate this by serially interrogating E-AB sensors by CV in undiluted serum in the presence and absence of saturating target concentrations (Figure 5). To achieve real-time visualization of these measurements, we adapted SACMES[33]—an open-source, Python-based script previously reported by our group—to the real-time processing of ΔE_p. This script continuously checks for the presence of new CV files in a computer folder, is able to calculate ΔE_p for any new file within milliseconds, and then graphs the data, thereby supporting real-time visualization (see Methods section for more details). To estimate the percentage contribution of sensor drift to our measurements, we calculated the signal change at every time point relative to the first measurement in each time course. The resulting graphs (Figure 5) show that, in the absence of a target, the three sensors display a continuous and slow (~0.08% min^{-1}) decrease in the peak-to-peak separation (~10% in 2 h). We attribute this drift to the progressive, nonspecific adsorption of serum proteins to the electrode surface, which can bring the redox reporter closer to the electrode surface thereby increasing the electron-transfer kinetics (and consequently decreasing ΔE_p). The addition of a target, in contrast, caused a sharp increase in electron-transfer rate that led to a steep drop in ΔE_p. For reasons we do not yet understand, E-AB signals in the bound state seem more stable in all cases, with drift rates approximately 1 order of magnitude below those seen in the absence of a target. Our results also demonstrate the reversibility of ΔE_p, which achieves almost a full recovery of the baseline signal (within 15% error) after a serum wash.

A critical point to consider when selecting the most suitable electrochemical interrogation technique for E-AB sensors is how the voltage program of that technique can affect the long-term sensor stability. The added value of CV over, for example, square wave voltammetry is that its linear voltage sweeps can be gentler on biosensor interfaces than differential voltage pulsing. To illustrate this beneficial effect, we compared the signal stability of tobramycin-detecting E-ABs under continuous electrochemical interrogation when using square wave voltammetry versus CV (Figure 6A). First, we observed that sensors that were serially interrogated by square wave voltammetry in PBS, every 5 s for 72 h (50,000 total measurements), underwent a 50% drop in peak current within the first 10 h (red trace in Figure 6A), followed by a more moderate but still progressive decrease (~0.4%·h^{-1}) down to only ~35% of the initial current. This degradation was completely eliminated when we repeated the experiment using

https://dx.doi.org/10.1021/acssensors.0c02455
ACS Sens. 2021, 6, 1199−1207

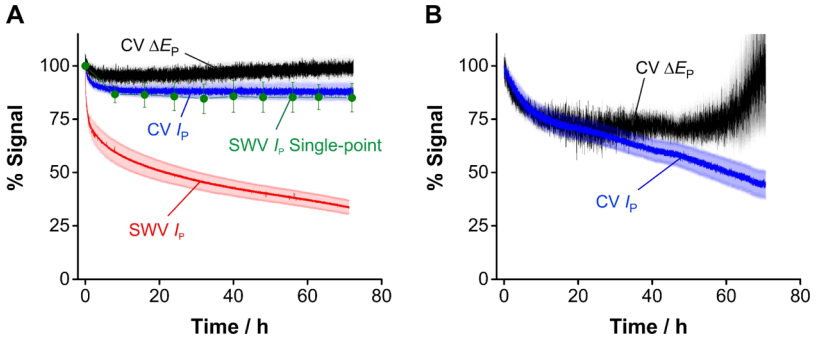

Figure 6. Long-term stability of E-AB sensors under different interrogation methods. (A) To investigate the extent to which continuously interrogating the sensors affects their operational stability, we interrogated E-AB sensors in PBS for 72 h by square wave voltammetry, either in continuous (5×10^4 scans) or single-point (10 scans) regimes, and by CV (7×10^4 scans) monitoring both peak-to-peak separation and the oxidation peak current. We observe that the continuous square wave voltammetry-based interrogation contributes to a fast loss in the signal (red trace), which dramatically decreases with less total measurements (at equal total experiment time, green circles). However, continuous CV-based interrogation (7×10^4 scans) by monitoring either ΔE_P or I_P does not contribute to the sensor signal loss. (B) When we switched to a more complex matrix such as undiluted serum, the CV-based interrogation presents an initial loss of signal (~15%) during the first 10 h likely due to monolayer reorganization, desorption, and the nonspecific binding of proteins. While CV peak currents continue to drop linearly after this initial decay (blue trace), ΔE_P remains constant for ~50 h, the point at which our software is no longer able to resolve voltammetric peaks from the charging current. These measurements were performed using tobramycin-binding E-AB sensors at controlled 25 °C and under continuous stirring. Shaded areas or error bars represent the standard deviation between the five electrodes.

a measurement frequency of one square wave voltammogram every 8 h (10 total measurements, green circles in Figure 6A), a clear indication that the measurement frequency contributes to the E-AB signal decay when using square wave voltammetry. The sensors serially interrogated by CV every 5 s (70,000 scans), in contrast, only showed a modest initial decrease in signal (~10% in either I_P or ΔE_P, blue and black traces in Figure 6A, respectively) over the first 5 h, which we attribute to the slow rearrangement or desorption of monolayer groups. This is in agreement with the changes in ΔE_P and I_P observed for both techniques when different aptamer coverages are used to fabricate sensors, demonstrating that ΔE_P-based interrogation is noticeably less sensitive to surface coverage variations (Figure S7 and Table S1). We speculate that the differences in the long-term performance of CV and SWV are due to the rapid, bidirectional voltage fluctuations occurring during the square wave interrogation that, as shown in previous works,[34,35] can cause field-induced oscillations of electrode-bound DNA molecules that may accelerate their desorption from the electrode surface. Our group has previously demonstrated that monolayer desorption plays a critical role in the E-AB signal drift;[22] thus, it is conceivable that interrogation approaches that heavily drive bidirectional DNA actuation may further contribute to the E-AB signal decay over time. In contrast, the uncharged, immobilized mercaptohexanol monolayer is less affected by these electric field-induced oscillations, which explains the negligible capacitive current changes occurring during the first 24 h of continuous interrogation by CV.[22]

The similar drift resistance of CV I_P and ΔE_P seen in PBS does not translate to unprocessed biological fluids, where ΔE_P outperforms I_P in long-term stability. This difference is revealed by repeating the CV experiment from Figure 6A in undiluted human serum (Figure 6B). Here, the initial decay accounts for ~25% signal loss during the first 10 h. We attribute this signal decrease, both in ΔE_P and I_P, to a combination of progressive monolayer desorption (both the blocking alkanethiols and aptamers)[22] and the nonspecific adsorption of serum proteins. Protein adsorption sterically pushes aptamer molecules closer to the electrode surface increasing E-AB electron-transfer kinetics, which we see in our measurements as a progressive decrease in ΔE_P. However, following this initial and rapid decay, I_P continues to linearly drop (~0.5%·h^{-1}) as monolayer elements continue to progressively desorb from the sensor surface, down to ~45% of the initial current at 60 h. ΔE_P measurements, in contrast, are less sensitive to monolayer desorption, presenting a stable response (~75% of initial value) for 50 h following the first decay. This drift resistance remains until the aptamer desorption is such that our data processing software becomes unable to find current peaks in the voltammograms. At that point, roughly 60 h after the beginning of the experiment, monolayer desorption is such that our software only visualizes the increasing capacitive current of the voltammograms.

One important advantage of the ΔE_P-based E-AB interrogation over square wave voltammetry is that ΔE_P presents less batch-to-batch and day-to-day variations in sensing performance in an unprocessed serum. To illustrate this effect, we serially interrogated three independent batches of six E-AB sensors each by square wave voltammetry (at the same square wave frequency and amplitude) in undiluted serum, every 5 s for 24 h on separate days, observing significant variability in peak currents (Figure 7A). Specifically, in the first 3 h of continuous measurements, one batch presented an initial signal decay of ~10% (green line) versus ~25% (blue line) for a second, while a third presented a current gain (gray line). Moreover, after the first 3 h the currents remained stable for one batch (blue line) but increased for the other two (green and gray lines). In contrast, interrogating three new batches using ΔE_P and a similar measurement rate, we observed identical signal behavior across batches and between days. For all three experimental repeats, we observed an initial decrease in the first few hours (as in Figure 6B), followed by a stable readout for about 18 h. These differences in baseline performance between techniques arise from the sensitivity of each technique toward changes in the sensing layer. While square wave voltammetry responds to both aptamer desorption from the sensor surface and nonspecific protein adsorption, ΔE_P-based interrogation is only sensitive to changes in electron transfer from the redox reporter and, therefore, only drifts with

https://dx.doi.org/10.1021/acssensors.0c02455
ACS Sens. 2021, 6, 1199−1207

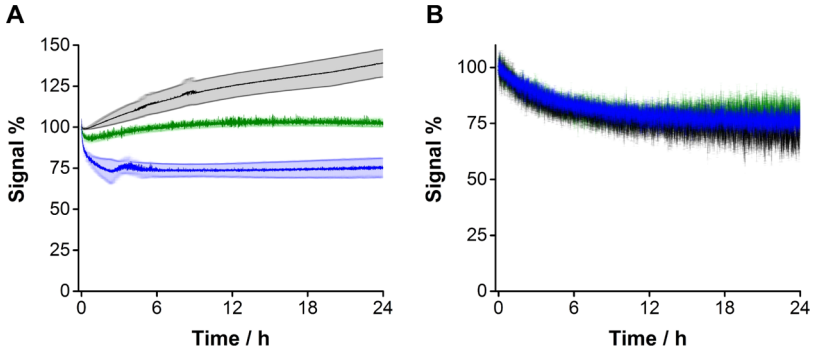

Figure 7. The batch-to-batch and day-to-day performance of E-AB sensors in undiluted serum is affected by the sensitivity of the interrogation method to changing sensor interfaces. (A) Square wave voltammetry-based measurements of E-AB peak current performed continuously every 5 s for 24 h. These measurements present significant variability in signal output between three batches of six sensors each (different colored traces), measured on three separate days. (B) The same variability is not seen for the ΔE_P-based interrogation, which produces indistinguishable traces between electrode batches and measurement days. Specifically, the initial decay in signal driven by monolayer reorganization and the nonspecific protein binding is identical between batches and, in all cases, it stabilizes at ~75% of its initial value. These measurements were performed using tobramycin-binding E-AB sensors at controlled 25 °C and under continuous stirring. Shaded areas represent the standard deviation between the five electrodes.

the sensor interface rearrangement seen during the first few hours of interrogation. This indicates that, in an analogous fashion to chronoamperometric current decays,[14] ΔE_P is insensitive to the number of aptamers on the sensor surface (within the range of packing densities studied in this work) and supports calibration-free measurements. In other words, once the monotonic relationship between ΔE_P and target concentrations for an E-AB type is established, this relationship can be used to determine target concentrations without the need to calibrate each individual sensor.

The work presented here is focused on the use of ΔE_P to interrogate E-AB sensors for the detection of small-molecule targets in biological media. However, we note the same interrogation approach can be readily applied to DNA-based sensors used in the detection of other target types and in different media, as long as the sensing mechanism involves binding-induced changes in reporter electron-transfer kinetics. For example, previous works have shown changes in ΔE_P upon hybridization of the surface-bound, MB-modified DNA with complementary strands.[36,37] In these cases, DNA hybridization moves MB further away from the electrode surface, leading to an increase in ΔE_P (i.e., signal-ON sensors). Similarly, the approach can be used to interrogate E-DNA sensors containing an antibody-binding epitope,[38] aptamer-based sensors binding to protein targets,[13] or DNA-origami-based sensors binding to single-entity, mesoscale targets.[39]

CONCLUSIONS

Method selection for the interrogation of E-AB sensors requires careful consideration of the intended application, the time resolution needed, and the importance given to the electrochemical information offered by different methods. We have previously discussed the advantages and disadvantages of many electrochemical methods,[19] mentioning in passing that CV is most often used for sensor characterization and not for interrogation. Here, however, we describe an approach to use CV for the direct interrogation of E-AB sensors, with the added benefit of retaining the rich electrochemical information provided by this technique. We have also adapted SACMES, a software we previously reported, to enable real-time, CV-based interrogation of E-AB sensors. The new version of the software (included as Supporting Information) allows tracking of voltammetric peak currents and voltages, ΔE_P, and arbitrary currents at user-specified voltages, continuously, and with millisecond processing speeds. Using this platform, we demonstrate that the peak-to-peak separation in cyclic voltammograms of E-AB sensors can be used to directly, rapidly, and reversibly interrogate this class of sensors. The method works across sensors binding to structurally different molecular targets and in complex media such as undiluted whole serum. Moreover, because ΔE_P is not a function of the moles of aptamer bound to the electrode surface but of the fractional populations of bound versus unbound aptamers, this parameter is drift-resistant and calibration-free and expands the operational lifetime of E-AB sensors relative to interrogation based on voltammetric peak currents. This approach supports fast, subsecond voltammetric measurements that could be valuable for the study of aptamer-target binding and dissociation kinetics or for the time-resolved study of dynamic processes in biological systems.

METHODS

Chemicals and Materials. PBS (11.9 mM HPO_3^{2-}, 137 mM NaCl, 2.7 mM KCl; pH = 7.4), sulfuric acid, sodium hydroxide, and procaine hydrochloride were purchased from Fisher Scientific (Waltham, MA). 6-Mercaptohexanol, tris(2-carboxyethyl)phosphine hydrochloride (TCEP), and the three nucleic acid aptamers were purchased from Sigma-Aldrich (St. Louis, MO). Human serum was purchased from BioIVT (Washington, D.C.). Tobramycin sulfate was purchased from GoldBio (St. Louis, MO). Vancomycin hydrochloride was purchased from Alfa Aesar (Ward Hill, MA). All solutions were prepared using ultrapure Milli-Q water with 18Ω resistance.

The nucleic acid aptamer sequences used in this work were obtained from previous works (see Table 1).

These sequences were purchased modified on the 5′end with hexanethiol and on the 3′end with MB and double HPLC purified. To

Table 1. Aptamer Sequences Used in This Work

target	sequence	refs
tobramycin	5′-GGG ACT TGG TTT AGG TAA TGA GTC CC-3′	3
vancomycin	5′-CGA GGG TAC CGC AAT AGT ACT TAT TGT TCG CCT ATT GTG GGT CGG-3′	32
procaine	5′-GAC AAG GAA ATC CTT CAA CGA AGT GGG TC-3′	17

https://dx.doi.org/10.1021/acssensors.0c02455
ACS Sens. 2021, 6, 1199−1207

prepare aptamer solutions for electrode modification, 1 μL of 100 μM of the modified sequences was incubated with 2 μL of 5 mM TCEP solution in water for 1 h to reduce the disulfide bonds. Then, we diluted the aptamer solutions in 1 mM 6-mercaptohexanol aqueous solution to a final aptamer concentration of 500 nM.

Electrochemical Measurements. Gold working (PN 002314, d = 1.6 mm) and coiled platinum wire counter electrodes (PN 012961) were purchased from ALS Inc. (Japan). Ag/AgCl (1 M KCl) reference electrodes (PN CHI111) were purchased from CH Instruments (USA). All the electrochemical measurements were carried out using a multichannel potentiostat CHI 1040C (CH Instruments). Cyclic voltammograms were recorded at different scan rates in the potential window from −0.5 to +0.1 V versus Ag/AgCl (1 M KCl). Square wave voltammograms were recorded from 0 to −0.5 V versus Ag/AgCl (1 M KCl) with an amplitude of 50 mV, a step size of 1 mV, and at 300 Hz. When specified, the temperature of the electrochemical cell was held constant by using a Huber Microprocessor Control water recirculation bath obtained from Huber (USA).

Electrode Modification. Gold electrodes were polished on a 1200/P2500 silicon carbide grinding paper (PN 36-08-1200, Buehler, USA) and on a cloth pad and alumina slurry (PN CF-1050, BASi, USA). After rinsing and sonicating them with water for 1 min to remove polishing debris, they were electrochemically activated by continuous cycles of CV from −0.3 to −1.6 V in 0.5 M NaOH and from 0 to 1.6 V in 0.5 M H_2SO_4, 250 times in each solution at a scan rate of 0.5 V/s. After this, the electrodes were rinsed with water and dipped in the aptamer−thiol mixture for 15 h at room temperature. After rinsing with water, the electrodes were ready for use. For the long-term stability experiments of Figures 6 and 7, we used a backfilling protocol to modify the electrodes. Briefly, we incubated the activated gold electrodes in 500 nM solutions of the MB-modified aptamer prepared in PBS for 2 h. After rinsing with deionized water, electrodes were dipped in 1 mM solution of 6-mercaptohexanol prepared in water for 15 h at room temperature. This backfilling protocol allowed us to increase the number of aptamer molecules immobilized on the electrode surface, from 0.9 ± 0.1 to 2.5 ± 0.1 pmol·cm^{-2}, obtaining larger voltametric peaks while decreasing the background current and without significantly affecting the ΔE_P signaling output (see Figure S8 and Table S2).

Data Analysis. To process the data obtained from the stability experiments where the sensors were continuously interrogated for long periods of time, we used a previously reported, open-source Python script called SACMES.[33] This software supports the real-time analysis, visualization, and control of electrochemical data with millisecond resolution, providing users the ability to extract peak currents (SWV, CV), peak-to-peak separation (CV), half-lives (chronoamperometry), and area under the curve (SWV, CV). Furthermore, this software provides the user with dynamic control over the smoothing and regression algorithms used to filter and fit the raw data.

The data obtained from all experiments were processed using data analysis software Origin Pro v8.5. Multipanel figures were assembled using Adobe Creative Cloud 2021.

■ ASSOCIATED CONTENT

Supporting Information

The Supporting Information is available free of charge at https://pubs.acs.org/doi/10.1021/acssensors.0c02455.

Study of the effect of the CV scan rate on dose−response curves, evaluation of peak broadening in CV with increasing scan rates, comparison of I_P and ΔE_P change for tobramycin sensors, evaluation of the precision of the CV-based method, calibration curve for procaine-binding E-AB sensors by SWV, evaluation of the response of sensors with different surface coverages, comparison of the electrochemical response of sensors prepared by a coimmobilization or a backfilling protocol, and Python script used for real-time data analysis (PDF)

■ AUTHOR INFORMATION

Corresponding Author

Netzahualcóyotl Arroyo-Currás − *Department of Pharmacology and Molecular Sciences, Johns Hopkins University School of Medicine, Baltimore, Maryland 21202, United States; Department of Chemical and Biomolecular Engineering, Whiting School of Engineering, Johns Hopkins University, Baltimore, Maryland 21218, United States; Institute for Nanobiotechnology, Johns Hopkins University, Baltimore, Maryland 21218, United States;* orcid.org/0000-0002-2740-6276; Phone: 443-287-4798; Email: netzarroyo@jhmi.edu

Authors

Miguel Aller Pellitero − *Department of Pharmacology and Molecular Sciences, Johns Hopkins University School of Medicine, Baltimore, Maryland 21202, United States;* orcid.org/0000-0001-8739-2542

Samuel D. Curtis − *Department of Pharmacology and Molecular Sciences, Johns Hopkins University School of Medicine, Baltimore, Maryland 21202, United States*

Complete contact information is available at: https://pubs.acs.org/10.1021/acssensors.0c02455

Author Contributions

M.A.P. and N.A.-C. designed all the experiments. M.A.P. fabricated E-AB sensors and performed all measurements included in this work. S.D.C. developed the numerical algorithm used for the real-time processing of voltammetric data. All authors contributed to the writing of this manuscript.

Notes

The authors declare no competing financial interest.

■ ACKNOWLEDGMENTS

N.A.-C. thanks the Oak Ridge Associated Universities for granting a 2019 Ralph E. Powe Junior Faculty Enhancement Award to support this work.

■ REFERENCES

(1) Fan, C.; Plaxco, K. W.; Heeger, A. J. Electrochemical interrogation of conformational changes as a reagentless method for the sequence-specific detection of DNA. *Proc. Natl. Acad. Sci. U.S.A.* **2003**, *100*, 9134−9137.

(2) Xiao, Y.; Lubin, A. A.; Heeger, A. J.; Plaxco, K. W. Label-Free Electronic Detection of Thrombin in Blood Serum by Using an Aptamer-Based Sensor. *Angew. Chem., Int. Ed.* **2005**, *44*, 5456−5459.

(3) Arroyo-Currás, N.; Somerson, J.; Vieira, P. A.; Ploense, K. L.; Kippin, T. E.; Plaxco, K. W. Real-time measurement of small molecules directly in awake, ambulatory animals. *Proc. Natl. Acad. Sci. U.S.A.* **2017**, *114*, 645−650.

(4) Schoukroun-Barnes, L. R.; Macazo, F. C.; Gutierrez, B.; Lottermoser, J.; Liu, J.; White, R. J. Reagentless, Structure-Switching, Electrochemical Aptamer-Based Sensors. *Annu. Rev. Anal. Chem.* **2016**, *9*, 163−181.

(5) Arroyo-Currás, N.; Dauphin-Ducharme, P.; Scida, K.; Chávez, J. L. From the beaker to the body: translational challenges for electrochemical, aptamer-based sensors. *Anal. Methods* **2020**, *12*, 1288−1310.

(6) Kang, D.; Zuo, X.; Yang, R.; Xia, F.; Plaxco, K. W.; White, R. J. Comparing the properties of electrochemical-based DNA sensors employing different redox tags. *Anal. Chem.* **2009**, *81*, 9109−9113.

(7) Kang, D.; Ricci, F.; White, R. J.; Plaxco, K. W. Survey of Redox-Active Moieties for Application in Multiplexed Electrochemical Biosensors. *Anal. Chem.* **2016**, *88*, 10452−10458.
(8) Lubin, A. A.; Plaxco, K. W. Folding-Based Electrochemical Biosensors: The Case for Responsive Nucleic Acid Architectures. *Acc. Chem. Res.* **2010**, *43*, 496−505.
(9) Schoen, I.; Krammer, H.; Braun, D. Hybridization kinetics is different inside cells. *Proc. Natl. Acad. Sci. U.S.A.* **2009**, *106*, 21649−21654.
(10) Vallée-Bélisle, A.; Plaxco, K. W. Structure-switching biosensors: inspired by Nature. *Curr. Opin. Struct. Biol.* **2010**, *20*, 518−526.
(11) Ferapontova, E. E.; Olsen, E. M.; Gothelf, K. V. An RNA Aptamer-Based Electrochemical Biosensor for Detection of Theophylline in Serum. *J. Am. Chem. Soc.* **2008**, *130*, 4256−4258.
(12) Somerson, J.; Plaxco, K. Electrochemical aptamer-based sensors for rapid point-of-use monitoring of the mycotoxin ochratoxin a directly in a food stream. *Molecules* **2018**, *23*, 912−919.
(13) Parolo, C.; Idili, A.; Ortega, G.; Csordas, A.; Hsu, A.; Arroyo-Currás, N.; Yang, Q.; Ferguson, B. S.; Wang, J.; Plaxco, K. W. Real-Time Monitoring of a Protein Biomarker. *ACS Sens.* **2020**, *5*, 1877−1881.
(14) Arroyo-Currás, N.; Dauphin-Ducharme, P.; Ortega, G.; Ploense, K. L.; Kippin, T. E.; Plaxco, K. W. Subsecond-Resolved Molecular Measurements in the Living Body Using Chronoamperometrically Interrogated Aptamer-Based Sensors. *ACS Sens.* **2018**, *3*, 360−366.
(15) Radi, A.-E.; Acero Sánchez, J. L.; Baldrich, E.; O'Sullivan, C. K. Reagentless, Reusable, Ultrasensitive Electrochemical Molecular Beacon Aptasensor. *J. Am. Chem. Soc.* **2006**, *128*, 117−124.
(16) Zhao, S.; Yang, W.; Lai, R. Y. A folding-based electrochemical aptasensor for detection of vascular endothelial growth factor in human whole blood. *Biosens. Bioelectron.* **2011**, *26*, 2442−2447.
(17) Downs, A. M.; Gerson, J.; Ploense, K. L.; Plaxco, K. W.; Dauphin-Ducharme, P. Sub-second-resolved Molecular Measurements Using Electrochemical Phase Interrogation of Aptamer-Based Sensors. *Anal. Chem.* **2020**, *92*, 14063−14068.
(18) Li, F.; Yu, Z.; Han, X.; Lai, R. Y. Electrochemical aptamer-based sensors for food and water analysis: A review. *Anal. Chim. Acta* **2019**, *1051*, 1−23.
(19) Pellitero, M. A.; Shaver, A.; Arroyo-Currás, N. Critical Review—Approaches for the Electrochemical Interrogation of DNA-Based Sensors: A Critical Review. *J. Electrochem. Soc.* **2020**, *167*, 037529.
(20) Santos-Cancel, M.; Lazenby, R. A.; White, R. J. Rapid two-millisecond interrogation of electrochemical, aptamer-based sensor response using intermittent pulse amperometry. *ACS Sens.* **2018**, *3*, 1203−1209.
(21) Arya, S. K.; Zhurauski, P.; Jolly, P.; Batistuti, M. R.; Mulato, M.; Estrela, P. Capacitive aptasensor based on interdigitated electrode for breast cancer detection in undiluted human serum. *Biosens. Bioelectron.* **2018**, *102*, 106−112.
(22) Shaver, A.; Curtis, S. D.; Arroyo-Currás, N. Alkanethiol Monolayer End Groups Affect the Long-Term Operational Stability and Signaling of Electrochemical, Aptamer-Based Sensors in Biological Fluids. *ACS Appl. Mater. Interfaces* **2020**, *12*, 11214−11223.
(23) Zhang, S.; Hu, R.; Hu, P.; Wu, Z.-S.; Shen, G.-L.; Yu, R.-Q. Blank peak current-suppressed electrochemical aptameric sensing platform for highly sensitive signal-on detection of small molecule. *Nucleic Acids Res.* **2010**, *38*, No. e185.
(24) Huang, K.-C.; White, R. J. Random Walk on a Leash: A Simple Single-Molecule Diffusion Model for Surface-Tethered Redox Molecules with Flexible Linkers. *J. Am. Chem. Soc.* **2013**, *135*, 12808−12817.
(25) Rowe, A. A.; Miller, E. A.; Plaxco, K. W. Reagentless Measurement of Aminoglycoside Antibiotics in Blood Serum via an Electrochemical, Ribonucleic Acid Aptamer-Based Biosensor. *Anal. Chem.* **2010**, *82*, 7090−7095.
(26) White, R. J.; Phares, N.; Lubin, A. A.; Xiao, Y.; Plaxco, K. W. Optimization of Electrochemical Aptamer-Based Sensors via Optimization of Probe Packing Density and Surface Chemistry. *Langmuir* **2008**, *24*, 10513−10518.
(27) Liu, Y.; Canoura, J.; Alkhamis, O.; Xiao, Y. Immobilization Strategies for Enhancing Sensitivity of Electrochemical Aptamer-Based Sensors. *ACS Appl. Mater. Interfaces* **2021**.
(28) Campos, R.; Kotlyar, A.; Ferapontova, E. E. DNA-Mediated Electron Transfer in DNA Duplexes Tethered to Gold Electrodes via Phosphorothioated dA Tags. *Langmuir* **2014**, *30*, 11853−11857.
(29) Campos, R.; Kékedy-Nagy, L.; She, Z.; Sodhi, R.; Kraatz, H.-B.; Ferapontova, E. E. Electron Transfer in Spacer-Free DNA Duplexes Tethered to Gold via dA10 Tags. *Langmuir* **2018**, *34*, 8472−8479.
(30) Laviron, E. General expression of the linear potential sweep voltammogram in the case of diffusionless electrochemical systems. *J. Electroanal. Chem. Interfacial Electrochem.* **1979**, *101*, 19−28.
(31) Dauphin-Ducharme, P.; Arroyo-Currás, N.; Adhikari, R.; Somerson, J.; Ortega, G.; Makarov, D. E.; Plaxco, K. W. Chain Dynamics Limit Electron Transfer from Electrode-Bound, Single-Stranded Oligonucleotides. *J. Phys. Chem. C* **2018**, *122*, 21441−21448.
(32) Dauphin-Ducharme, P.; Yang, K.; Arroyo-Currás, N.; Ploense, K. L.; Zhang, Y.; Gerson, J.; Kurnik, M.; Kippin, T. E.; Stojanovic, M. N.; Plaxco, K. W. Electrochemical Aptamer-Based Sensors for Improved Therapeutic Drug Monitoring and High-Precision, Feedback-Controlled Drug Delivery. *ACS Sens.* **2019**, *4*, 2832−2837.
(33) Curtis, S. D.; Ploense, K. L.; Kurnik, M.; Ortega, G.; Parolo, C.; Kippin, T. E.; Plaxco, K. W.; Arroyo-Currás, N. Open Source Software for the Real-Time Control, Processing, and Visualization of High-Volume Electrochemical Data. *Anal. Chem.* **2019**, *91*, 12321−12328.
(34) Rant, U.; Arinaga, K.; Scherer, S.; Pringsheim, E.; Fujita, S.; Yokoyama, N.; Tornow, M.; Abstreiter, G. Switchable DNA interfaces for the highly sensitive detection of label-free DNA targets. *Proc. Natl. Acad. Sci. U.S.A.* **2007**, *104*, 17364−17369.
(35) Rant, U.; Arinaga, K.; Tornow, M.; Kim, Y. W.; Netz, R. R.; Fujita, S.; Yokoyama, N.; Abstreiter, G. Dissimilar Kinetic Behavior of Electrically Manipulated Single- and Double-Stranded DNA Tethered to a Gold Surface. *Biophys. J.* **2006**, *90*, 3666−3671.
(36) Yang, W.; Lai, R. Y. Comparison of the Stem-Loop and Linear Probe-Based Electrochemical DNA Sensors by Alternating Current Voltammetry and Cyclic Voltammetry. *Langmuir* **2011**, *27*, 14669−14677.
(37) Lai, R. Y.; Walker, B.; Stormberg, K.; Zaitouna, A. J.; Yang, W. Electrochemical techniques for characterization of stem-loop probe and linear probe-based DNA sensors. *Methods* **2013**, *64*, 267−275.
(38) Kang, D.; Parolo, C.; Sun, S.; Ogden, N. E.; Dahlquist, F. W.; Plaxco, K. W. Expanding the Scope of Protein-Detecting Electrochemical DNA "Scaffold" Sensors. *ACS Sens.* **2018**, *3*, 1271−1275.
(39) Arroyo-Currás, N.; Sadeia, M.; Ng, A. K.; Fyodorova, Y.; Williams, N.; Afif, T.; Huang, C.-M.; Ogden, N.; Andresen Eguiluz, R. C.; Su, H.-J.; Castro, C. E.; Plaxco, K. W.; Lukeman, P. S. An electrochemical biosensor exploiting binding-induced changes in electron transfer of electrode-attached DNA origami to detect hundred nanometer-scale targets. *Nanoscale* **2020**, *12*, 13907−13911.

https://dx.doi.org/10.1021/acssensors.0c02455
ACS Sens. 2021, 6, 1199−1207